Tuning Pt and Cu sites population inside functionalized UiO-67 MOF by controlling activation conditions

UNIVERSITÀ DEGLI STUDI DI TORINO

Tuning Pt and Cu sites population inside functionalized UiO-67 MOF by controlling activation conditions

L. Braglia,[a,b] E. Borfecchia,[a] K. A. Lomachenko,[b] A. L. Bugaev,[a,b] A. A. Guda,[b] A. V. Soldatov,[b] B. T. Lønstad-Bleken,[c] S. Øien-Ødegaard,[c] U. Olsbye,[c] K. P. Lillerud,[c] S. Bordiga,[a,c] G. Agostini,[d,e] M. Manzoli[f] and C. Lamberti[b,g]

[a.] *Department of Chemistry, NIS Interdepartmental Centre and INSRM reference centre, University of Turin, via Quarello 15A, I-10135 Turin, Italy.*
[b.] *IRC "Smart Materials", Southern Federal University, Zorge Street 5, 344090 Rostov-on-Don, Russia.*
[c.] *inGAP Centre for Research Based Innovation, Department of Chemistry, University of Oslo, Oslo, Norway.*
[d.] *European Synchrotron Radiation Facility (ESRF), Avenue des Martyrs 71, 38000 Grenoble, France.*
[e.] *Leibniz Institute for Catalysis at the University of Rostock (LIKAT), Albert-Einstein-Str. 29A, D-18059 Rostock, Germany.*
[f.] *Department of Drug Science and Technology, NIS Interdepartmental Centre, University of Torino, Via P. Giuria 9, 10125 Torino, Italy.*
[g.] *Department of Chemistry, CrisDi Interdepartmental Centre and INSRM reference University of Turin, via Pietro Giuria 7, 10125 Turin, Italy*

Abstract
The exceptional thermal and chemical stability of UiO-66, -67 and -68 class of isostructural MOFs [*J. Am. Chem. Soc*., 2008, **130**, 13850] makes them ideal materials for functionalization purposes aimed in introducing active centres for potential application in heterogeneous catalysis. We previously demonstrated that a small fraction (up to 10%) of the linkers in the UiO-67 MOF can be replaced by bipyridine-dicarboxylate (bpydc) moieties exhibiting metal-chelating ability and enabling the grafting of Pt(II) and Pt(IV) ions in the MOF framework [*Chem. Mater*., 2015, **27**, 1042] upon interaction with $PtCl_2$ or $PtCl_4$ precursors. Herein we extend this functionalization approach into two directions. First, we show that controlling the activation of the UiO-67-Pt we can move from a material hosting isolated Pt(II) sites anchored to the MOF framework with Pt(II) exhibiting two coordination vacancies (potentially interesting for C−H bond activation) to the formation of very small Pt nanparticles hosted inside the MOF cavities (potentially interesting for hydrogenation reactions). The second direction consists in the extension of the approach to the insertion of Cu(II), obtained via interaction with $CuCl_2$, and exhibiting interesting red-ox properties. All materials have been characterized by in situ X-ray absorption spectroscopy at the Pt L_3- and Cu K-edges.

1. Introduction

Metal-organic frameworks (MOFs) are crystalline, porous solids consisting of metal ions or clusters, coordinated with organic molecules. The large number of combinations for inorganic and organic building units offers an almost infinite variety of structural solutions with a wide range of properties.[1-7] An additional degree of freedom consists in the functionalization of the MOFs frameworks that further extend the range of possibly obtainable structures.[8-14] Since about one decade, MOFs are considered as potential candidates as shape-selective heterogeneous catalysts for reactions running at mild conditions.[15-24]

As the metal sites in the cornerstones of most of the MOF structures show at maximum one coordination vacancy (see e.g. the HKUST-1[25-27] and the CPO-27, or MOF-74,[28-31] cases), non-functionalized MOFs have limited application in catalysis, where at least two coordination vacancies are required on the active site. Consequently, functionalization represents an attractive way to introduce active sites in MOFs structures.

The recently discovered UiO-66, -67 and -68 classes of iso-structural MOFs are obtained connecting $Zr_6O_4(OH)_4$ inorganic cornerstones with 1,4-benzene-dicarboxylate (bdc), 4,4'biphenyl-dicarboxylate (bpdc) or or 4,4'-terphenyl-dicarboxylate (tpdc) linkers, for the UiO-66, UiO-67 and UiO-68 MOFs, respectively [32-34]. Due to their outstanding stability at high temperatures, high pressures and in presence of different solvents, these materials are among the few MOFs already commercialized for potential applications in the fields of catalysis, gas storage, and gas purification. For the same reasons the UiO-66, -67 and -68, family has already been subjected to several functionalization procedures, involving both the $Zr_6O_4(OH)_4$ inorganic cornerstone and the organic linkers, as well as intentionally toned defect insertion.[35-38] As far as the inorganic cornerstone functionalization is concerned, Zr atoms have been partially or totally substituted with Hf[39, 40] or Ce[41-44] atoms. Substitution with cerium allows to play with the Ce(IV) $\leftrightarrow$ Ce(III) redox chemistry providing some reactivity to the cornerstone. Coming to the linker functionalization, several routes have been undertaken, including: (i) grafting of $-NH_2$, $-NO_2$, -Br groups σ-bonded to the bdc ring;[45-49] grafting of $Cr(CO)_3$ complexes π-bonded to the bdc ring;[50] (iii) encapsulation of Pt,[51, 52] Pd,[53, 54] Au,[55] AuPd,[56] Ru,[57] Ag,[58] metal-nanoparticles (NPs) inside the tetrahedral and octahedral MOF cavities.. Moreover, for UiO-67, the substitution of a small fraction of bpdc linkers by bipyridine-dicarboxylate (bpydc) moieties, exhibiting metal-chelating ability, enables the path for post-synthetic grafting of metal ions in the MOF framework upon interaction with metal precursors.[51, 59, 60]

Herein we extend this functionalization approach into two directions. First, tuning the H_2 flow during the activation procedure of the UiO-67-Pt we can move from a material hosting isolated framework Pt(II) exhibiting two coordination vacancies (potentially interesting for C−H bond activation) to the formation of very small Pt NPs hosted inside the MOF cavities (potentially interesting for hydrogenation reactions). The second direction consists in the extension of the approach to the insertion of Cu(II), obtained via interaction with $CuCl_2$, and exhibiting interesting red-ox properties already evidenced in other Cu-containing MOFs.[61-63]

The fact that MOFs are mainly constituted by low Z elements (C, O, N, H) implies that they are almost transparent to hard X-rays;[64, 65] this allows to collect, at the metal K- or L-edges, high quality transmission X-ray absorption spectra characterized by an optimized edge jump $\Delta\mu x$ as high as 1.0-1.5, resulting in accurate data, analyzable up to 15-20 $Å^{-1}$ (vide infra Figure 3a). This makes X-ray absorption techniques both in the extended X-ray absorption fine structure (EXAFS) and X-ray absorption near edge structure (XANES) a technique of choice in characterizing the electronic and structural configuration of metal centers hosted in MOF structures, as testified by many studies.[28, 29, 32-34, 40, 48, 59, 64, 66-90] In this study we have

characterized Pt- and Cu-functionalized UiO-67 MOFs via in situ X-ray absorption spectroscopy at the Pt L_3- and Cu K-edges, respectively.

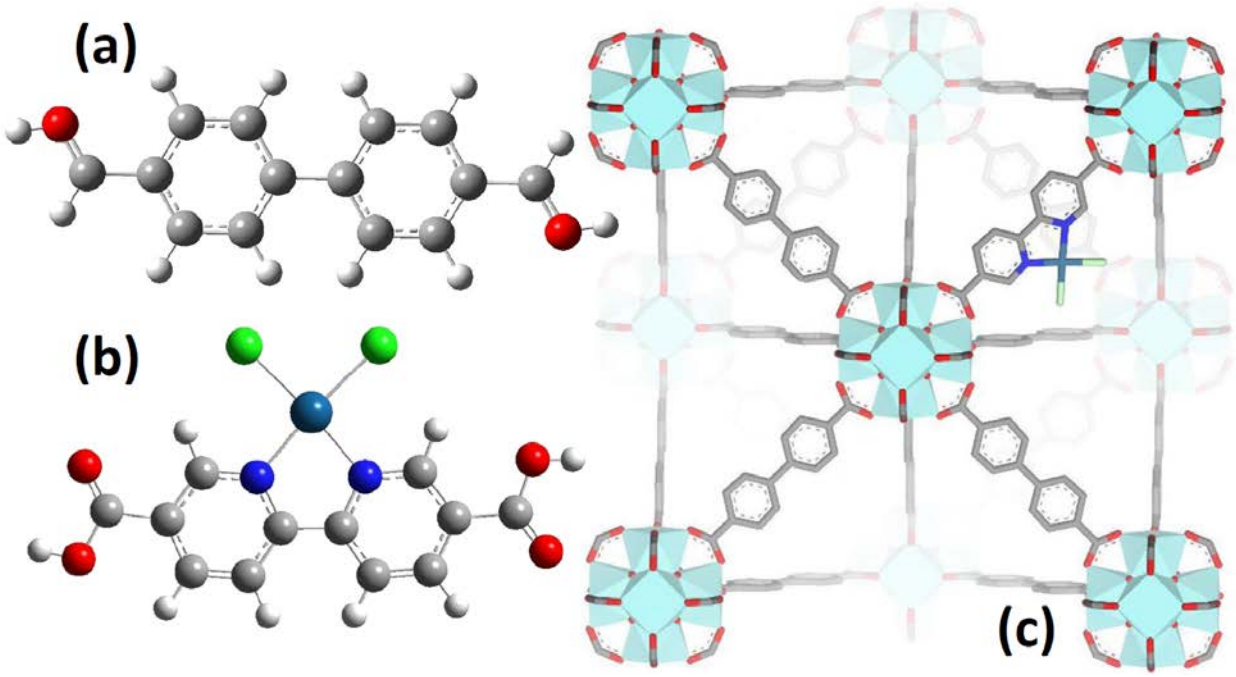

Figure 1. Part (a): structure of the standard bpydc linker used for the synthesis of the non-functionalised UiO-67 MOF. Part (b): structure of the (H_2bpydc)$PtCl_2$ linker inserted in the UiO-67 structure showing 2 N and 2 Cl in the first coordination shell of Pt(II) and showing the distortion induced on the two rings by N/C substitution and Pt insertion. Part (c) three-dimensional representation of Pt(II)-functionalized UiO-67 MOF. Colour code: H white, C grey, N blue, O red, Cl green, Pt cyan. Previously unpublished figure.

2. Experimental and methods

2.1. Materials

All chemicals were used as received. $ZrCl_4$ (Sigma) must be dry and of high purity for successful synthesis.

2.1.1. Synthesis of 2,2'-bipyridine-5,5'-dicarboxylic acid

In a 25 mL beaker glass, 6.0 g $HNO_{3\,(aq)}$ (65 %) was slowly added to 9.0 mL deionized water to obtain 26 % wt. HNO_3. 1.50 g 5,5'-dimethyl-2,2'-bipyridine was added and quickly dissolved in the acid. The solution was transferred to a 25 mL Teflon-lined autoclave which was heated to 160 °C and kept at that temperature for 16 hours. The autoclave was allowed to slowly cool to room temperature before opening. A crystalline, weakly yellow powder was isolated by filtration and then washed 5 times with approximately 50 mL portions of water. The filtrate was cooled to 0 °C and carefully brought to pH 7 by addition of saturated $NaHCO_3$ solution, at which a weakly yellow precipitate was formed. This solid was isolated by filtration and washed in the same manner as above. ^{1}H-NMR confirmed the two solids were both pure H_2bpydc. The yield was 1.74 g (92 %).

Crystals of H_2bpydc suitable for single crystal XRD were obtained directly from the autoclave. A complete data set was acquired on a Bruker D8 Venture equipped with a Photon 100 detector and using Mo Kα radiation (λ = 0.71073 Å). Data reduction was performed with the Bruker Apex3 Suite, the structure was solved with ShelxT[91] and refined with ShelxL.[92] Olex2 was used as user interface.[93] The H_2bpydc molecules form 1D H-bonded chains analogous to the previously reported structure,[94] but the packing mode is slightly different.

2.1.2. Synthesis of UiO-67-bpy($PtCl_2$) by postsynthetic modification

116 µL (6.5 mmol) H_2O, 502 mg (2.15 mmol) $ZrCl_4$ and 2.63 g (21.5 mmol) benzoic acid was added to 50 mL of DMF in a beaker glass, and the mixture was stirred until a clear solution was obtained. It was then heated to 120 °C while stirring gently. 469 mg (1.94 mmol) H_2bpdc and 110 mg (0.22 mmol) $PtCl_2$(H_2bpydc) was then added, a clear, yellow solution was quickly obtained. The solution was transferred to a round-bottom flask and kept at 120 °C for 72 hours while stirring in a reflux apparatus. A colorless powder was isolated by filtration, then immediately suspended in 20 mL fresh DMF while still wet. The suspension was kept at 100 °C while stirring to extract unreacted precursor and modulator from the pores. The powder was isolated by filtration, washed twice with 15 mL portions of hot DMF (100 °C), 5 times with 30 mL portions of dry acetone, then dried in air at 150 °C. The yield was 718 mg (94 %).

To a solution of 100 mg K_2PtCl_4 in 20 mL DMF, the entire sample was submerged and kept at 100 °C for 24 hours while stirring (20 % molar excess of Pt to bpy sites). A bright yellow powder was isolated by filtration, washed twice with 15 mL portions of hot DMF (100 °C), 5 times with 30 mL portions of dry acetone, then dried in air at 150 °C. The yield was 770 mg (> 99 %).

2.1.3. Synthesis of UiO-67-bpy(CuOHCl) by postsynthetic modification

The starting UiO-67-bpy MOFs were synthesized by standard solvothermal method, as described in more details in previous studies,[59] by reacting $ZrCl_4$ with different mixtures of H_2bpdc and H_2bpydc linkers (10% wt. of bpydc) in a solution of dimethylformamide (DMF). 5 molar equivalents of benzoic acid were added to obtain a modulator effect, which resulted in a porous MOF with monodispersed particles and well-defined crystallinity.[95] The Cu-functionalized Cu-UiO-67-bpy derivatives were prepared employing a post synthesis modification approach, by submerging the MOF powder in solutions of $CuCl_2$ dihydrate in 2-propanol, and heating the solution at reflux conditions for one hour. The resulting bright green powders were washed in three cycles with 2-propanol

2.2. Pt L_3- and Cu-k edges XAS data collections, EXAFS data analysis

Pt L_3-edge (11560 eV) and Cu-K edge (8990 eV) XAS data were collected at the I811 beamline of the Max Lab II source (Lund, Sweden).[96] Max Lab II was operating at 1.5 GeV with a uniform current between 250 and 100 mA. The white beam produced by a liquid He-cooled superconducting wiggler was monochromatized by a horizontally sagitally focused double-crystal Si(111) monochromator. At the Cu K-edge the monochromator was detuned to 20% to minimize the third harmonic, while this procedure is not needed at the Pt L_3-edge. Spectra were

collected in transmission mode using 30 cm ionization chambers for I_0 and I_1; the intensity I_2 transmitted by a Pt (or Cu) reference foil located after the sample was measured using a photodiode, and the resulting spectrum employed for energy alignment purpose.
All XAS spectra were measured employing a home-made cell allowing sample activation in temperature and gas dosage under *in situ* or *operando* conditions,[97] monitoring the evolution of the XAS features while controlling temperature and gas feed. The XAS data reduction and EXAFS extraction procedure was performed using the Athena codes.[98] The parametric EXAFS data analysis was performed with IFEFFIT[99] code that employs phases and amplitudes computed by FEFF6 code.[100, 101] as detailed elsewhere.[59]

2.3. Pt L_3-edge XANES simulations

For all clusters simulating the local environments of Pt atoms hosted inside UiO-67-Pt MOF and successive modification by chemical reactivity with H_2, Br and thiol, the ground-state electronic structures and atomic geometries were calculated using hybrid DFT B3LYP level of theory[102] using the ADF-2015 program package.[103, 104] The QZ4P basis set was used in all calculations. Thus, each atomic orbital was represented as a combination of four Slater type orbitals with different exponential powers and four polarization functions. Molecular orbitals of the 2p core level and unoccupied levels were used to calculate dipole matrix elements, and Lorentzian convolution is subsequently applied for comparison with experiment. For the DFT-MO calculations shown in the main text, we first obtain eigenvalues and corresponding wave functions. The matrix elements are then evaluated for transitions between 2p core level and unoccupied MOs using dipole transition operators. In order to compare with experimental XANES spectra, a convolution of calculated matrix elements was performed with a Lorentzian profile using energy-dependent line width. In the pre-edge region, the width of the Lorentzian profile corresponds to a core hole lifetime broadening for Co. This value is then increased in higher energy interval with a smooth arctangent function. The parameters of the matrix elements calculations (grid step, size number of unoccupied MOs) and energy convolution are fixed once for all complexes. The DFT-MO calculated spectra were subsequently aligned according to the energy value of the Pt 2p orbital, thus reproducing the chemical shift for different species. A rigid shift with the identical was applied for all spectra in order to align the energy scale between experimental data and theoretical calculations.

3. Results and discussion

3.1. Pt-functionalization of UiO-67 MOF: state of the art

Introducing a chemically active Pt site as part of the UiO-67 framework is of great interest as platinum has rich redox chemistry, showing 0, II and IV stable oxidation states. Moreover, certain square planar Pt(II) coordination complexes are known to be active in C-H bond activation,[105] see the scheme reported in Figure 1b,c. In particular, the dichlorobipyrimidyl platinum(II), $PtCl_2$(BPYM), performs the catalytic oxidation in fuming or concentrated sulfuric acid, achieving high yields of methanol with selectivity higher than 90%.[106, 107] It is consequently

of potential interest to investigate the possibility to heterogenize such process anchoring the active Pt(II) complex on some high surface area material such as recently shown by the group of Schüth, for polymers first[108, 109] and for N-doped carbons[110] successively or as done mere recebntly by Øien et al.[59] who have succeeded in functionalizing UiO-67 with (H_2bpydc)$PtCl_2$ or (H_2bpydc)$PtCl_4$ units, substituting 10% of the standard bpdc linkers. The authors used EXAFS, XANES and valence-to-core resonant inelastic X-ray scattering techniques to prove the insertion of Pt atoms in the expected framework position of UiO-67, see Figure 1c.

Using EXAFS and XANES, the local coordination environment and the oxidation state of Pt can be monitored under *in situ* conditions. The elimination of chloride ligands from Pt in a continuous gas flow of diluted H_2 (3% H_2 in He) have been monitored by EXAFS during temperature ramping, Figure 2a. The spectrum collected at room temperature (black curve) exhibits both the first shell Pt-N and the Pt-Cl contributions centred around 1.5 and 1.9 Å, phase uncorrected Fourier transform (FT), highlighted by vertical blue and green dashed lines, respectively. Upon increasing the temperature, both contributions decrease in intensity because of the increased Debye-Waller factors (σ^2_N and σ^2_{Cl}). Starting from about 600 K the Pt-Cl contribution shows a much more relevant decrease in temperature than the Pt-N one, suggesting that the system starts loosing chlorine ligands. A standard EXAFS analysis failed because of the high correlation between the coordination numbers ($N_{Pt–N}$; $N_{Pt–Cl}$) and the thermal parameters (σ^2_N; σ^2_{Cl}).[59] The problem was solved performing a complex data analysis briefly summarized hereafter.

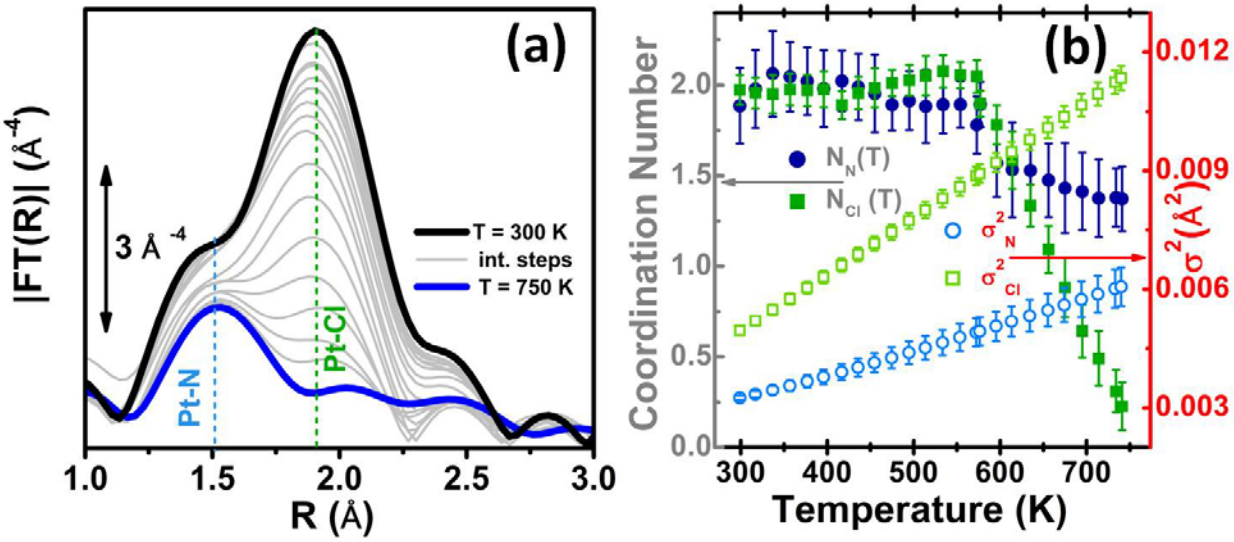

Figure 2. Part (a): k^3-weighted, phase uncorrected, FT of Pt L_3-edge EXAFS spectra collected during the in situ H_2-TPR experiments on $PtCl_2$(H_2bpydc) functionalized UiO-67-Pt(II) MOF in the 300 K (black spectrum) – 750 K (blue spectrum) range performed with diluted H_2 flow (3% H_2 in He). Part (b): quantitative data analysis of the set of spectra shown in part (a) by modelling the temperature dependence of the Debye-Waller factors (σ^2_N and σ^2_{Cl}) based on the Einstein model. Previously unpublished figure replotting data published in Ref. [59].

First, we worked only on the sub-set of data in the interval between RT and 473 K. In this temperature range no bond breaking occurs so that it was possible to fix $N_N = N_{Cl} = 2$. On that sub-set of in situ EXAFS data they performed a parametric refinement, commonly adopted in XRPD Rietveld refinements,[111, 112] adopting the Einstein model to describe the temperature dependence of both σ^2_N and σ^2_{Cl} factors. The Einstein model approximates the vibrational density of states as a Dirac delta function spiked at a single frequency named Einstein frequency (ω_E). The model assumes that the pairs Pt–N (or Pt–Cl) behaves as a quantum harmonic oscillator of mass equal to the reduced mass of the atomic pair (M = 13.070 and 30.004 amu for the Pt–N and Pt–Cl pairs, respectively). Under such assumptions, the $\sigma^2(T)$ behaviour is straightforwardly determined by the only ω_E parameter according to the equation (1):[59, 113]

$$\sigma^2(T) = \frac{\hbar}{M\omega_E} cotgh\left[\frac{\hbar\omega_E}{2k_BT}\right] = \frac{\hbar^2}{Mk_B\Theta_E} cotgh\left[\frac{\Theta_E}{2T}\right] \qquad (1)$$

Being Θ_E the Einstein temperature of the Pt–N (or Pt–Cl) bond, related to the Einstein frequency by the relationship: $\hbar\omega_E = k_B\Theta_E$, where $\hbar = 1.055 \times 10^{-34}$ J s is the reduced Plank constant and $k_B = 1.38 \times 10^{-23}$ J K^{-1} is the Boltzmann constant.

This approach allowed us to reduce the number of parameters used to optimize the thermal factors of the series from ~40 to only two, Θ_E(Pt–N) and Θ_E(Pt–Cl), with a consequent reduction of the correlation among the optimized parameters and thus a reduction of the relative error bars. Once obtained the Einstein temperatures Θ_E(Pt–N) = (709 ± 63) K and Θ_E(Pt–Cl) = (333 ± 9) K, the dependence of both σ^2_N and σ^2_{Cl} vs. T was straightforwardly obtained via Eq. (1) and extrapolated on the whole set of data (i.e. also above 473 K). This strategy allowed to have stable fits in the whole temperature range while optimizing both N_N and N_{Cl}, as shown in Figure 2b. From this data analysis, it is evident that both N_N and N_{Cl} are stable to the stoichiometric values of 2.0 up to 575 K, when they start to decrease together. However, while N_{Cl} decreases almost linearly to 0.4 at 750 K, N_N undergoes a fast decrease to 1.6 at 610 K and then remains almost stable, being its value at 750 K of 1.4. This means that a prolonged activation in H_2 of the UiO-67-Pt(II)_PMLS MOF in the 610-640 K interval will result in a minimal loss of Pt(II), that will lose the Pt–N connection with the framework, but in the break of an important fraction of the Pt–Cl bonds. The experiment reported in Figure 2 proved that this activation temperature interval is ideal to obtain a material where most of the functionalized Pt(II) species are still linked to the MOF framework, exhibiting the coordination vacancies needed to make the UiO-67-Pt(II) material a potential heterogeneous catalyst.[59] The presence of coordination vacancies at platinum sites was also directly testified by IR spectroscopy of adsorbed CO. No evidence of Pt-Pt signal of aggregate platinum phase was observed in the experiment reported in Figure 2.

EXAFS was also used to prove the high reactivity of such coordinatively unsaturated Pt(II) species. We followed the liquid-phase ligand exchange with toluene-3,4-dithiol (H_2tdt) and the

liquid-phase oxidative addition of Br_2 to Pt, see Figure 3. All the observed reactions take place without any degradation of the framework, as testified by parallel XRPD experiments.

Also the XANES part of the XAS spectrum is sensitive to the changes undergone by the local environment of Pt(II) along the chemical reactions reported in Figure 3. Indeed, upon change in the Pt oxidation state, Pt L_3-edge XANES will show a very small edge shift while it will exhibit a noticeable variation of the intensity of the "white-line" peak.[59, 114-116] Indeed, the XANES part of the Pt L_3-edge mainly derives from the promotion of core $2p_{3/2}$ electrons into empty $5d_{3/2}$, $5d_{5/2}$ and 6s valence states, so manly probing the unoccupied density of 5d-states and partially 6s-states. The XANES spectra reported in Figure 4a for UiO-67-Pt(II) MOF before (red line) and after interaction with H_2tdt (blue line) and Br_2 (green line) clearly follow this phenomenological trend. In particular, interaction with H_2tdt (blue spectrum in Figure 4a) does not affect the white line intensity, affecting only the post edge and EXAFS region of the spectrum; on these basis it was concluded that we are in the presence of a ligand exchange reaction where two Cl ligands are exchanged with the two S atoms of the bulky H_2tdt unit. Conversely, interaction with Br_2 (green spectrum in Figure 4a) results in a significant increase in the white line intensity, testifying an oxidation process from Pt(II) to Pt(IV).[59, 116]

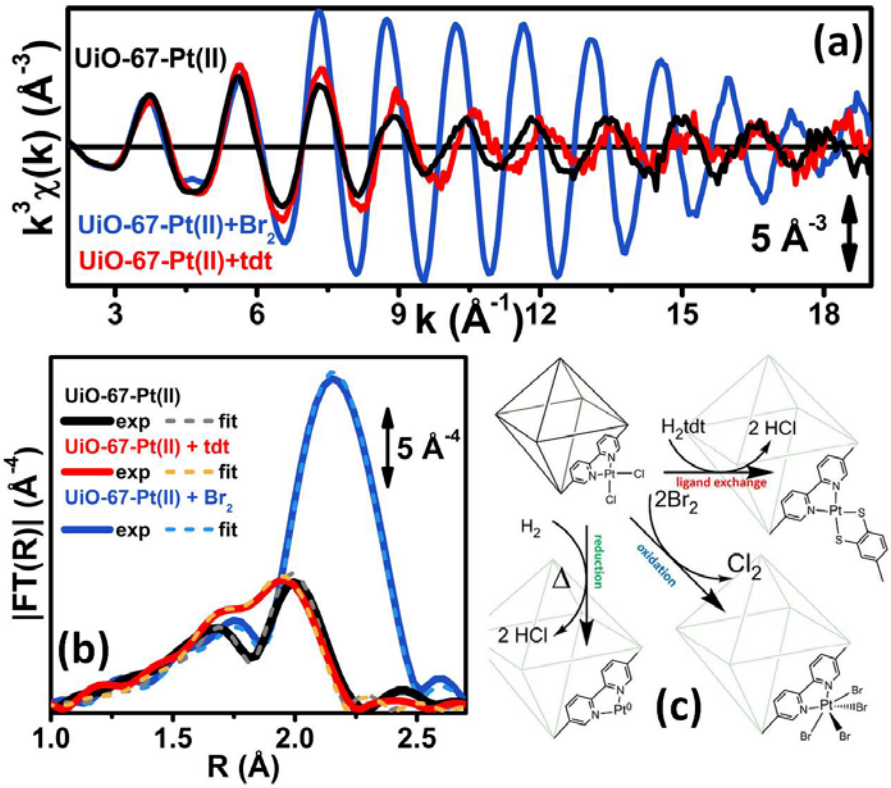

Figure 3. Part (a): experimental Pt L_3-edge $k^3\chi(k)$ spectra of UiO-67-Pt(II) before (black line) and after interaction with H_2tdt (red line) and Br_2 (blue line). Part (b): modulus of the k^3-weighted, phase uncorrected FT of the experimental EXAFS spectra reported in part (a), solid lines, same color code as in part (a). The corresponding best fits are also reported, as dashed lines of similar colour. Part (c): Schematic representation of the reactivity of Pt(II) species in functionalized UiO-67-Pt MOFs that has been highlighted in the EXAFS and XANES study reported in

Figure 2 and in parts (a,b) of this figure. The sketched square bi-pyramid represents the octahedral large cavity of UiO-67, measuring about 16 Å in diagonal.[32, 34] Previously unpublished figure replotting data published in Ref. [59].

On a more quantitative ground, the simulation of the XANES spectra, performed with the ADF code[103, 104] on the H_2bpydcPtCl$_4$, H_2bpydcPtCl$_2$, H_2bpydcPt-tdt and H_2bpydcPtBr$_4$ molecular fragments (Figure 4b), were able to reproduce correctly the variation of the white line intensity, and post edge features.[116] The data reported in Figure 4 testifies the potentialities of the XANES simulations.[117]

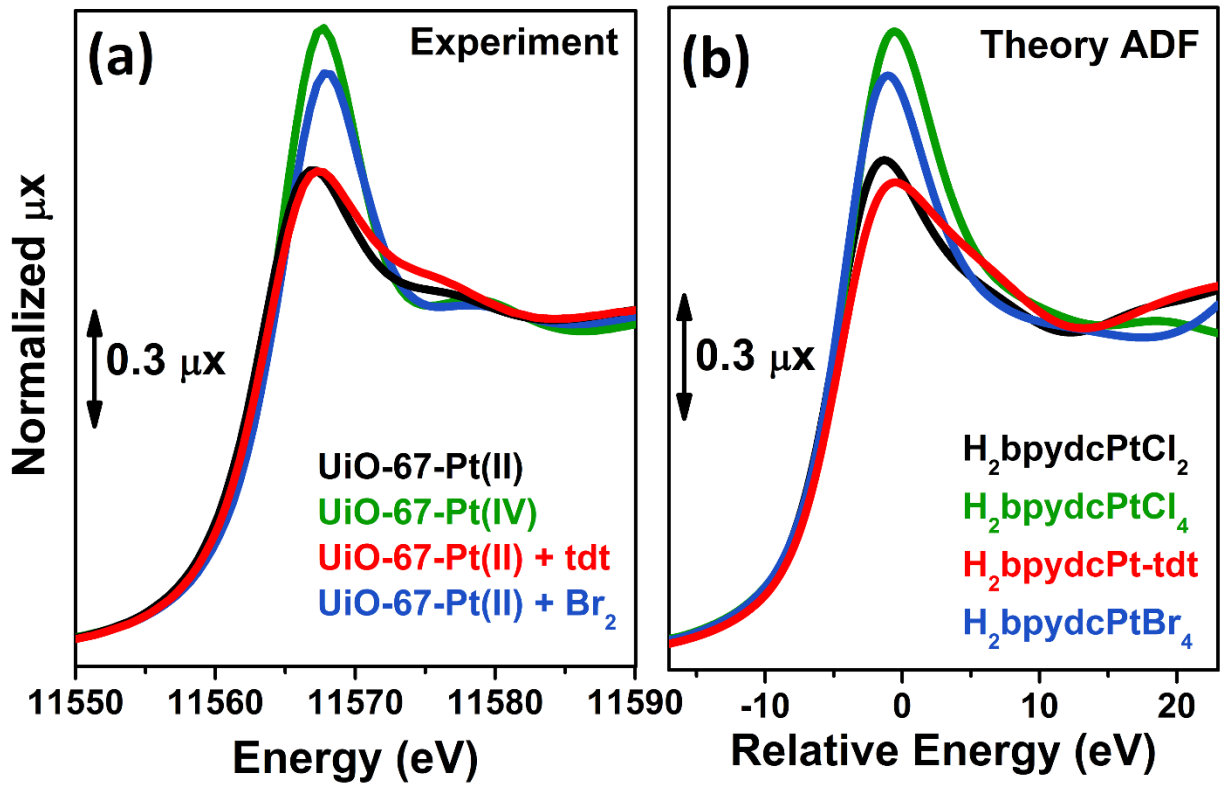

Figure 4. Part (a): experimental Pt L_3-edge XANES spectra of UiO-67-Pt(VI) (green) and of UiO-67-Pt(II) before (red line) and after interaction with H_2tdt (blue line) and Br_2 (green line). Part (b): As part (a) for the theoretical spectra computed with ADF code.

3.2. Tuning the Pt sites population inside UiO-67-Pt MOF by controlled H_2-TPR

The interesting results obtained by us in the Pt-functionalisation of UiO-66 (here summarized in Section 3.1), together with the relevance of hosting reactive metal NPs inside the MOF cavities, [51-58] encouraged us to investigate different activation conditions in order to be able to tune the population of Pt phases inside functionalised UiO-67, from isolated Pt(II) sites anchored to the MOF framework with Pt(II) exhibiting two coordination vacancies (potentially interesting for C−H bond activation) to small Pt NPs (potentially interesting for hydrogenation reactions).

In the following two subsections, we reports the XANES and EXAFS results, and the corresponding data analysis, obtained by thermal activation of functionalised UiO-67-Pt MOF

under inert flow (He, 3.2.1) and under concentrated H_2 flow (10% H_2 in He, 3.2.2). In both cases the EXAFS data have been analysed using a parametric refinement allowing us to obtain, along the activation procedure, the first shell Pt coordination numbers ($N_{Pt–N}$, $N_{Pt–Cl}$ and, when present $N_{Pt–Pt}$) with the minimal correlation possible with the corresponding Debye-Waller parameters. From such data, the fractions of the different platinum phases present in the sample have been obtained, as outlined hereafter. The following nomenclature has been adopted for the different relative fractions of Pt species formed in the experiments: f_{bpyCl2} corresponds to Pt atoms coordinated to the bpydc linker in the MOF framework, still containing the Cl ligands; f_{bpy} stands for Pt atoms coordinated to the bpydc linker in the MOF framework after the loss of two Cl ligands; f_{extra} represents non-aggregated extra-framework Pt atoms; and f_{NPs} stands for extra-framework Pt atoms aggregated in NPs. While f_{bpyCl2}, f_{bpy} and f_{NPs} fractions corresponds to well defined Pt species, f_{extra} does not. Although it is fully reasonable to infer that, once the Pt–N bonds with the framework are broken, Pt atoms will behave as isolated species for a while before being incorporated into a pre-existing NP (or before interacting with other isolated Pt atoms to produce a new NP), the local environment of such Pt species is very difficult to be predicted. Most probably such Pt atoms will experience a large variety of different local environments resulting in an average contribution to the measured EXAFS spectrum that is very low because of heterogeneity. This fact has been very well documented by EXAFS studies on Fe-substituted zeolites showing that the amplitude of the experimental EXAFS signal is strongly dumped once Fe atoms migrates form framework into extra-framework sites,[118-120] contributing only in the very short *k*-range (typically up to 6 $Å^{-1}$).

3.2.1. Thermal activation of UiO-67-Pt under inert atmosphere.

Figure 5a,b reports the evolution of the Pt L_3-edge XANES and EXAFS spectra during in situ thermal activation of the functionalized UiO-67-Pt MOF under inert He flow in the 300–750 K range. The evolution of both XANES and EXAFS spectra observed under inert flow is very similar to what observed working under diluted H_2 flow,[59] see Figure 2a for the EXAFS part. Also in this case we did not observe any evidence of Pt–Pt bond in the FT of the EXAFS data (Figure 5b), evidencing the absence of formation of Pt metal NPs. According to this evidence, the fractions of the remaining three Pt phases are obtained as follows:

$$f_{NPs} = 0; \qquad f_{bpyCl2} = N_{Cl}/2; \qquad f_{extra} = (2 - N_N)/2; \qquad f_{bpy} = 1 - f_{bpyCl2} - f_{extra} \qquad (2)$$

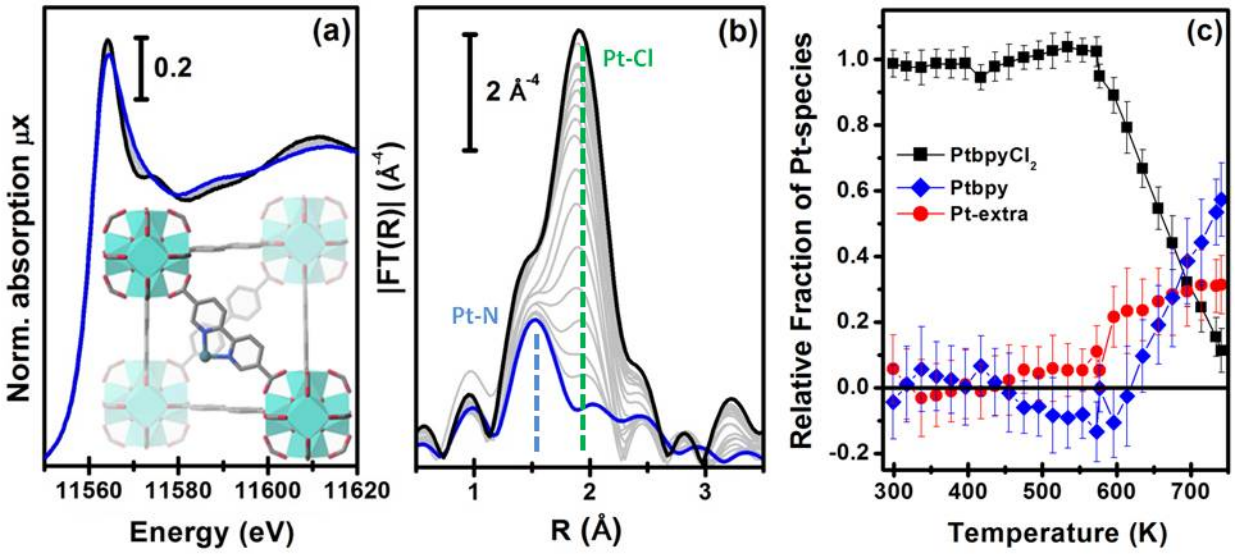

Figure 5. Part (a): Evolution of the Pt L_3-edge XANES spectra during in situ thermal activation of the functionalized UiO-67-Pt MOF under inert He flow in the 300–750 K range. The inset reports a cartoon description of the dominant final phase (framework-coordinated Pt atom that has lost the two Cl ligands). Part (b): as part (a) for the k^3-weighted, phase uncorrected, FT of the corresponding EXAFS data. Also highlighted with blue and green dashed lines are the typical positions of the Pt–N and Pt–Cl contributions, respectively. Part (c): fraction of the different Pt phases present in the sample, estimated from the $N_{Pt–N}$ and $N_{Pt–Cl}$ coordination numbers obtained from the parametric refinement of the whole set of EXAFS data, according to the assumptions reported in Eqs. (2).

The analysis of the evolution during the activation experiment of the relative fractions of the different Pt phases performed according to Eqs (2) is reported in Figure 5c. Till 550 K, within the experimental errors, $f_{bpyCl2} = 1$ and $f_{extra} = f_{bpy} = 0$. Then, f_{bpyCl2} starts to rapidly decrease down to 0.1, in an almost linear fashion with the increasing temperature; an opposite trend is observed for f_{bpy}, reaching 0.6 at 750 K, while f_{extra} exhibits an abrupt increase at ca. 570 K, and subsequently stabilizes around 0.3.

3.2.2. Thermal activation of UiO-67-Pt under concentrated H_2 flow.

Evolution of the Pt L_3-edge XANES and EXAFS spectra during in situ H_2-TPR experiment of the $PtCl_2(H_2bpydc)$ functionalized UiO-67-Pt(II) MOF performed in concentrated H_2 flow (10% H_2 in He) is reported in parts (a) and (b) of Figure 6, respectively. In this case, the experiment consists in a linear temperature increase up to 625 K with a heating ramp of 5 K min^{-1}, followed by almost 3 h in isotherm, see the open grey triangles in Figure 6c.

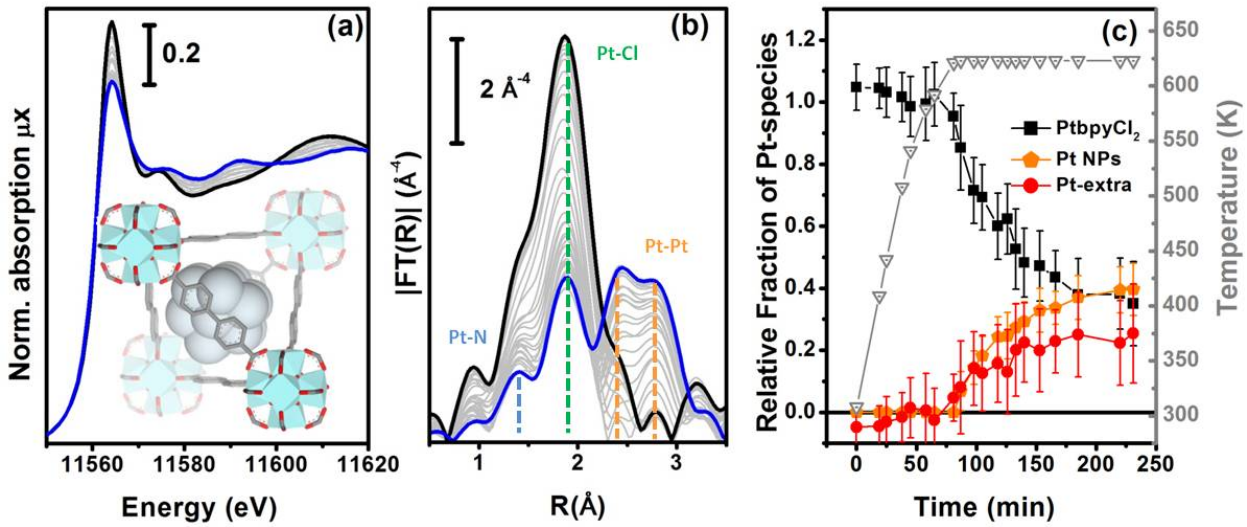

Figure 6. Part (a): Evolution of the Pt L_3-edge XANES spectra during in situ H_2-TPR experiment of the $PtCl_2(H_2bpydc)$ functionalized UiO-67-Pt(II) MOF performed in concentrated H_2 flow (10% H_2 in He). The inset reports a cartoon description of the dominant final phase (metal NPs). Part (b): as part (a) for the k^3-weighted, phase uncorrected, FT of the corresponding EXAFS data. Also highlighted with blue, green and orange dashed lines are the typical positions of the Pt–N, Pt–Cl and Pt–Pt contributions, respectively. Part (c), full black, red and orange symbols, left ordinate axis: fraction of the different Pt phases present in the sample, estimated from the $N_{Pt–N}$, $N_{Pt–Cl}$ and $N_{Pt–Pt}$ coordination numbers obtained from the parametric refinement in the whole set of EXAFS data, according to the assumptions reported in Eqs. (5). Part (c), open grey triangles, right ordinate axis: evolution of the sample temperature with time, highlighting the linear increase up to 625 K in 65 min followed by 2 h 55 min in isotherm.

Differently to what observed in the previous cases, where $N_{Pt–Cl}$ started to decrease significantly before $N_{Pt–N}$, in the present case both $N_{Pt–N}$ and $N_{Pt–Cl}$ remain, within the associated error bars, equal to 2 during the whole heating ramp up to 625 K (indicating $f_{bpyCl2} = 1$) and start to decrease in the same way during the isotherm (data not reported for brevity). This indicates that, under concentrated H_2 flow, when framework Pt(II) species loss the Pt–Cl bond they almost simultaneously loss also the Pt–N bond and thus the connectivity with the MOF framework, thus becoming extra-framework species. Based on this evidence, we can assume $f_{bpy} = 0$, while f_{bpyCl2} can be determined averaging the contribution of both Pt–Cl and Pt–N bonds: $f_{bpyCl2} = (N_{Cl}/2 + N_N/2)/2$.

A second important difference, very evident in Figure 6b, is the structured signal in the 2.5–4.0 Å range, typical of the single and multiple scattering Pt–Pt contributions of the fcc metal phase, testifying the formation of Pt NPs. Hence, the EXAFS data analysis also provides a first shell $N_{Pt–Pt}$ coordination number. Unfortunately the fraction of Pt atoms in the NPs phase cannot be straightforwardly deduced from the $N_{Pt–Pt}$ number obtained from the EXAFS data analysis, because the average coordination number of a fcc NP increases with the particle size, asymptotically reaching the value of 12 of the bulk.[121-125] Consequently, the $N_{Pt–Pt} \leftrightarrow f_{NPs}$ relationship can be established only if the particle size distribution has been determined by an independent SAXS[126-133] or a TEM[74, 124, 133-135] study.

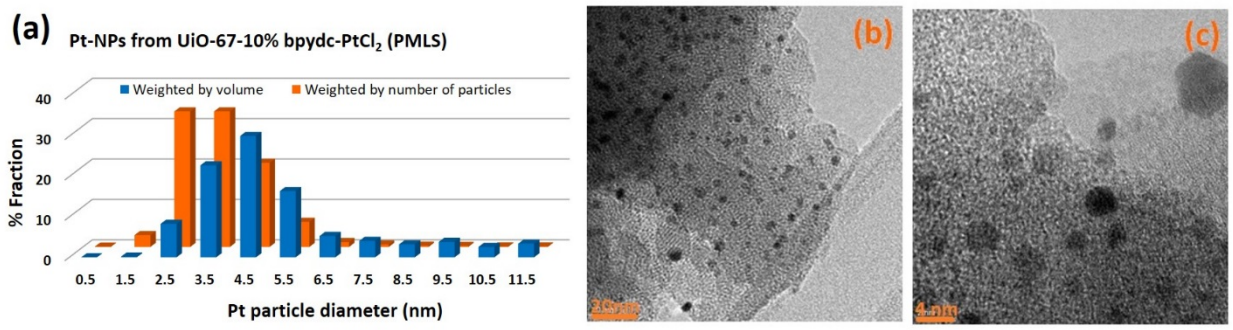

Figure 7. Part (a): Pt NP distributions (weighted by particle number (orange) or by volume (blue): $w_P(d_i)$ and $w_V(d_i)$, respectively, see Eq. (3)) obtained from the TEM analysis on the $PtCl_2(H_2bpydc)$ functionalized UiO-67-Pt(II) MOF measured after the H_2-TPR XAS experiment reported in Figure 6. Parts (b) and (c) reports a selection of two micrographs at different magnifications.

Consequently, at the end of the H_2-TPR experiment reported in Figure 6, the sample was cooled down to 300 K in He flow, recovered and subjected to a TEM study (see Figure 7b,c for two selected micrographs taken at different magnification), that resulted in the particle size distribution $w_P(d_i)$ reported in Figure 7a (orange bars) and obtained selecting the NP in 12 classes of amplitude 1 nm. $w_P(d_i)$ reports the fraction of NP that have a diameter d falling in the class centred in d_i and results in an average NP diameter of $\langle d \rangle_P$ = 3.5 nm with a standard deviation of 1.2 nm. The orange NP distribution $w_P(d_i)$ is the standard output from a TEM analysis, but is however not the correct one to be used to extrapolate the average coordination number measured in the EXAFS study. Indeed, the measured EXAFS signal is the average signal coming from all the Pt atoms in the sample. This means that a large particle contributes more to the EXAFS signal than a small one, because it contains more atoms. The orange $w_P(d_i)$ distribution, weighted by particles, has to be corrected by weighting for the corresponding volume fraction into $w_V(d_i)$ defined as follows:

$$w_V(d_i) = \frac{4\pi}{3V}(\frac{1}{2}d_i)^3 w_P(d_i), \text{ where: } V = \sum_{i=1}^{n} \frac{4\pi}{3}(\frac{1}{2}d_i)^3 w_P(d_i) \qquad (3)$$

The volume-weighted NP distribution, obtained from $w_P(d_i)$ via Eq. (3), is reported in Figure 7a (orange bars) and results in an average NP diameter of $\langle d \rangle_V$ = 5.5 nm with a standard deviation of 1.5 nm. Comparing $w_P(d_i)$ and $w_V(d_i)$, the more important role played by the high-d region is evident. Knowing the average coordination number of an fcc NP with given diameter, $N(d_i)$, the volume-weighted NP distribution allows us to obtain the average coordination number of the whole particle distribution estimated from the TEM analysis (N_{TEM}) as:

$$N_{TEM} = \sum_{i=1}^{n} N(d_i) w_V(d_i) = 10.9 \qquad (4)$$

Once N_{TEM} has been determined, the fraction of Pt atoms occurring as NPs is obtained as $f_{NPs} = N_{Pt}/N_{TEM}$, while the fraction of Pt atoms in non-aggregated extra-framework position is obtained as complement to unit from the sum of the other two fractions. Summarizing:

$$f_{bpy} = 0; \qquad f_{bpyCl2} = (N_{Cl}/2 + N_N/2)/2; \qquad f_{NPs} = N_{Pt}/N_{TEM}; \qquad f_{extra} = 1 - f_{bpyCl2} - f_{NPs} \qquad (5)$$

The evolution of the relative fractions of the different Pt-phases during in situ H_2-TPR experiment in concentrated H_2 flow is summarized in Figure 6c. The weakness of this approach consists in the fact that we assume the same NP size distribution along the whole H_2-TPR experiment. Nonetheless, this approach provides a correct evaluation of f_{NPs} for the last points of the treatment, that is the needed information in the view of potential application in catalysis.

Within the experimental error, along the whole heating ramp up to 625 K, Pt atoms maintains the same square planar coordination with two nitrogen and two chlorine ligands in their first coordination shell. During the isotherm, they break simultaneously the bonds with both the Cl ligands and MOF framework, becoming extra-framework species, that progressively aggregates into NPs. After 3 h of isotherm at 625 K the distribution among the different Pt phases reaches an asymptotic equilibrium.

3.3. Structure and red-ox properties of isolated Cu sites in UiO-67-Cu MOF

The interesting results obtained on the Pt-functionalised UiO-67 MOF encouraged us to extend the study using other metals. Because of its interesting red-ox chemistry, our first choice was on copper. We consequently prepared a Cu-functionalized UiO-67 MOF by consisting in contacting the bpydc-containing UiO-67-bpy MOF with a $CuCl_2$ dihydrate precursor.[60] The synthesis method succeeded in grafting isolated Cu(II) ions on the functionalised bpydc linkers of the UiO-67 framework but, contrary to what expected, the local environment of copper was not composed by two nitrogen and two chlorine atoms as was the case for the Pt-functionalised MOF, see Figure 1b,c.

Indeed, just from a first simple comparison of the XANES (Figure 8a) and EXAFS (Figure 8b) data collected on as-prepared UiO-67-Cu (black) and on the tBbpyCuCl_2 model compound (green, where Cu(II) is in square planar geometry coordinating 2N and 2 Cl atoms, see Figure 8c) clearly testifies that the local environment of Cu atoms in the two materials is significantly different. The EXAFS data clearly shows a lack of EXAFS signal in the (1.5 – 2.1) Å region in the MOF, suggesting the presence of only one Cl atom in the first coordination shell of the Cu(II).

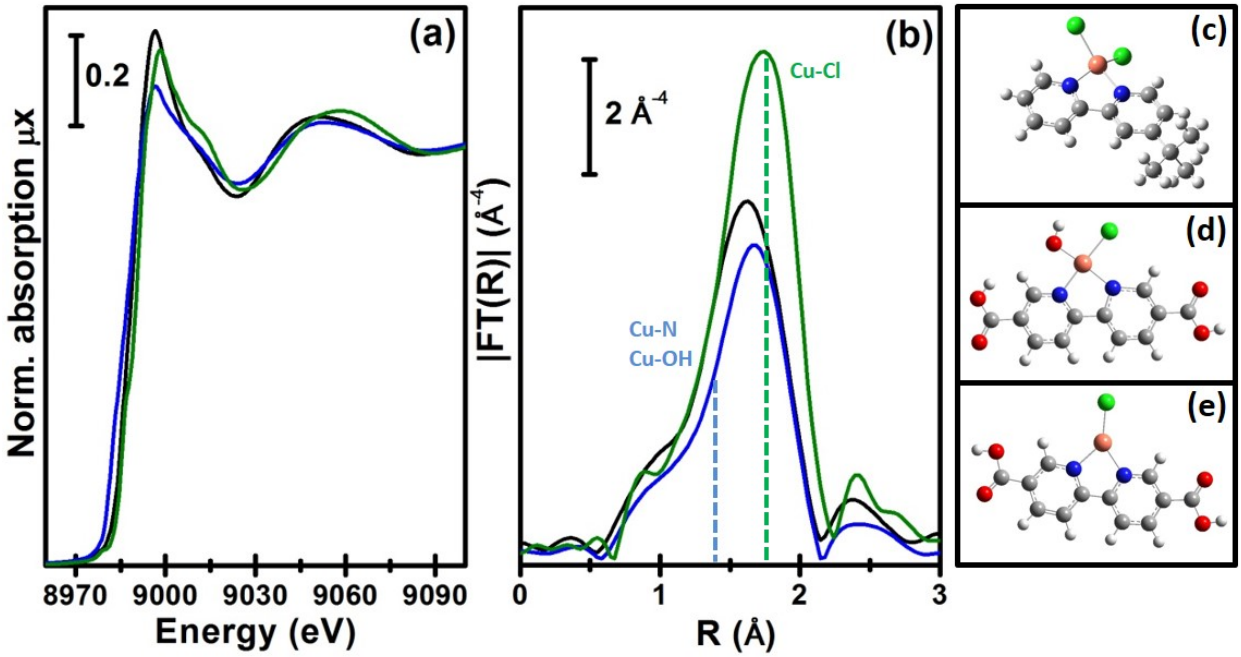

Figure 8. Part (a): Cu K-edge XANES spectra of tBbpyCuCl$_2$ model compound (green) and of UiO-67-Cu MOF before and after the in situ thermal activation in N_2 flow (black and blue spectra, respectively). Part (b): as part (a) for the k^3-weighted, phase uncorrected, FT of the corresponding EXAFS data. Also highlighted with blue and green dashed lines are the typical positions of the (Cu–N or Cu-OH) and Cu–Cl contributions, respectively. Part (c) structure of the tBbpyCuCl$_2$ model compound as obtained from the single-crystal XRD refinement (data collected at 100 K). Parts (d) and (e): DFT-optimized structures for the Cu(II)ClOH(H_2bpydc) and Cu(I)Cl(H_2bpydc) complexes used as starting point for the EXAFS fits of the UiO-67-Cu MOF before and after the in situ thermal activation. Atom colour code: Cu: orange; O: red; N: blue; Cl: green, C: gray; H: white. Previously unpublished figure reporting spectra and structures from Ref.[60]

Figure 9 reports the XANES spectra (part a) and the k^3-weighted, phase uncorrected (part b), FT EXAFS spectra for the exemplificative case of UiO-67-Cu during the thermal treatment in inert gas flow, from RT (as-prepared state, black) to 523 K (blue). Spectra collected at intermediate temperatures are also reported, as gray thin lines.

The XANES spectrum for the as-prepared material is characterized by the absence of any defined pre-edge/edge peaks, and by a rather intense white line feature at ~ 8996.6 eV, typical of Cu(II) centres coordinated to water molecules and, eventually, OH groups.[136-141] As also supported by the comparison with the tBbpyCuCl$_2$ model compound, the overall shape and the edge energy position in the XANES of the as-prepared material are consistent with a 2+ oxidation state of copper. The spectral changes observed during thermal activation involve a clear decrease of the white line feature, accompanied by a significant shift of the absorption edge towards lower energies (ca. 3.6 eV, as evaluated by monitoring the energy position of the first main maximum of the first derivative spectra.[142, 143] At the end of the heating ramp, a shoulder starts to be distinguishable in the XANES edge-rising region at ca. 8983 eV, falling in an energy range typical of two- or three-coordinated Cu(I) sites.[144, 145] These evidences suggest a ligand loss process associated to the reduction of the starting Cu(II) sites into Cu(I), as thermal treatment proceeds. Such spectral modifications are also accompanied by the sample color change from green to light-green/white as the temperature increases, supporting the formation of coordinatively unsaturated Cu(I) sites after mild thermal treatment in inert atmosphere.

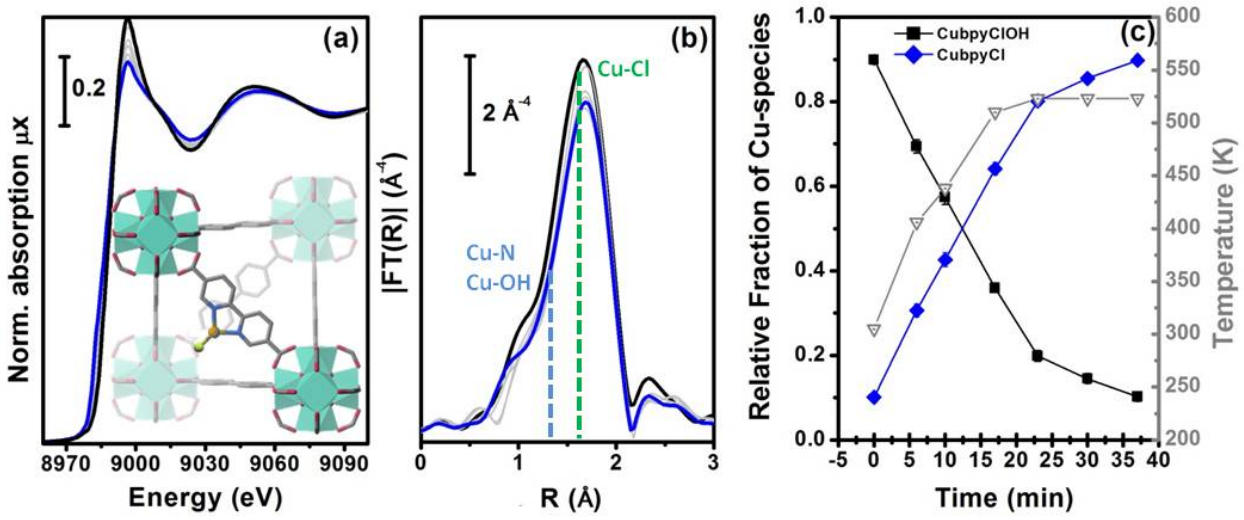

Figure 9. Part (a): Evolution of the Cu K-edge XANES spectra during the in situ thermal activation in N_2 flow of the CuClOH(H_2bpydc) functionalized UiO-67-Cu(II) MOF in the 300–523 K range. The inset reports a cartoon description of the dominant final phase (framework-coordinated Cu(I) species with a Cl ligand). Part (b): as part (a) for the k^3-weighted, phase uncorrected, FT of the corresponding EXAFS data. Also highlighted with blue and green dashed lines are the typical positions of the (Cu–N or Cu–OH) and Cu–Cl contributions, respectively. Part (c), full black and blue symbols, left ordinate axis: fraction of the different Cu phases present in the sample estimated according to a linear combination of the XANES spectra of the starting and final phases. Part (c), open grey triangles, right ordinate axis: evolution of the sample temperature with time, highlighting the linear increase up to 523 K in 23 min followed by 13 min in isotherm. Previously unpublished figure reporting spectra from Ref.[60]

We succeeded in reproducing the EXAFS and XANES spectra of the as prepared UiO-67-Cu MOF using as starting model that obtained from the optimization of the [Cu(II)(bpydc)(OH)Cl] complex (see Figure 8d) at the DFT level of theory with VASP 5.3 code,[146, 147] using a kinetic energy cut-off for the plane-wave basis set of 400 eV. The EXAFS-optimized distances were: $R_{Cu–OH}$ 1.91 ± 0.01 Å, $R_{Cu–N}$ = 2.026 ± 0.006 Å and $R_{Cu–Cl}$ = 2.265 ± 0.006 Å, in reasonable agreement with the DFT-optimized ones.[60] The same holds for the DFT-optimized [Cu(I)(bpydc)Cl] complex (see Figure 8e), that allowed to correctly reproduce the EXAFS spectrum of the N_2-activated UiO-67-Cu MOF, resulting in $R_{Cu–N}$ = 1.989 ± 0.008 Å and $R_{Cu–Cl}$ = 2.249 ± 0.007 Å. The progressive evolution from the [Cu(II)(bpydc)(OH)Cl] complex into the [Cu(I)(bpydc)Cl] complex upon thermal activation in inert atmosphere has been quantified by linear combination of the XANES spectra and reported in Figure 9c.

Further insights in the nature and reactivity of these [Cu(I)(bpydc)Cl] complexes, representing an interesting plat-form for future experiments on Cu(I)-catalyzed reactions, were achieved by monitoring with XAS and FTIR the interaction of the thermally-treated material with the CO probe molecule. Both techniques pointed out the efficient and reversible formation Cu(I)-mono-carbonyl adducts with CO, compatible with [Cu(I)(bpydc)(CO)Cl] species as highlighted by EXAFS fitting.

The overall picture is confirmed by XANES simulations performed with the FDMNES code[117] for the key experimental conditions investigated, including as-prepared MOFs in air, after thermal treatment in N_2-flux and upon interaction with CO.[60]

4. Conclusions

A post-synthesis functionalisation approach has been sucesfully emploied to graft Pt(II) and Cu(II) atoms on UiO-67 MOF functionalized with 10% of bpydc ligands. The *in situ* EXAFS analysis, for all the series of samples at RT, demonstrates that the Pt atoms are grafted to the bpydc-linkers in squared planar coordination with two Cl and two N atomic neighbors. XAS spectroscopy was used in operando conditions to study the activation of UiO-67-Pt functionalized MOFs, demonstrating that, tuning the activation conditions, two types of catalytically active sites can be formed in the cavities of the MOF: (i) isolated, highly uncoordinated framework >Pt(II) species bond to the two N atoms of the to the functionalising bpydc linkers of the MOF and (ii) and Pt NPs. XAS was used for monitoring the temperature-dependent behavior of UiO-67-Pt during thermal activation process, in different gas feeds (0%H_2/He, 3%H_2/He and 10%H_2/He). EXAFS analysis of the data collected during operando H_2-TPR was performed using the Einstein model to predict the temperature dependence of the Debye-Waller factors and to reduce the correlation among optimized parameters. In 10% H_2/He flow, EXAFS clearly show the loss of both Cl and N scattering contributions, while the rising of an intense signal at around 2.7 Å, associated to the Pt-Pt contributions, unambiguously indicates Pt-NPs formation. Conversely, in pure He flow, the only significant change observed during TPR is the progressive decrease of the Pt-Cl single scattering contribution, leading to the conclusion that the Pt grafted to the bpydc-linkers remains naked. In general, Pt sites in UiO-67 Pt-MOFs tend to form Pt-NPs in presence of H_2 and to remain naked, but still grafted to the bpydc-linkers, in inert gas flow. This study demonstrate two families of different catalytic active Pt sites can be generated in UiO67-Pt MOF by properly tuning the activation conditions. In situ IR, ex situ TEM and catalytic tests support the operando XAS study.

By combining *in situ* and *operando* XAS and FTIR spectroscopies, we assessed the successful incorporation of well-defined Cu complexes in the UiO-67 framework in form of Cu(II)ClOH(H_2bpydc) complex, that evolve into Cu(I)Cl(H_2bpydc) upion thermal acrivatiion in inert atmosphere. We explored local coordination geometry, redox properties and reactivity of the dominant Cu species formed in different conditions relevant to potential future applications in catalysis. EXAFS fits and XANES simulations, based on DFT-optimized geometries, yielded detailed structural and electronic information on the major Cu-species formed.

The methodology of post-synthesis functionalisation of UiO-67 MOF, here described for $PtCl_2$ and $CuCl_2$ has been recently successfully extended using $RhCl_3$ and $IrCl_3$ precursors, while a first attempt to insert of gold via $HAuCl_4$ as precursors failed.[148]

Acknowledgments

LB, KAL, ALB, AAG, AVS and CL acknowledge the Megagrant of the Russian Federation Government to support scientific research at the Southern Federal University, no. 14.Y26.31.0001. Authors are grateful to MAX-lab for the allocation of the beam time (proposal 20140449) and to Dr. Stefan Carlson for the technical support during the experiments at the I811 beamline.

Notes and references

1. S. L. James, *Chem. Soc. Rev.*, 2003, **32**, 276-288.
2. J. L. C. Rowsell and O. M. Yaghi, *Microporous Mesoporous Mat.*, 2004, **73**, 3-14.
3. G. Ferey, *Chem. Soc. Rev.*, 2008, **37**, 191-214.
4. N. Stock and S. Biswas, *Chem. Rev.*, 2012, **112**, 933-969.

5. T. R. Cook, Y. R. Zheng and P. J. Stang, *Chem. Rev.*, 2013, **113**, 734-777.
6. H. Furukawa, K. E. Cordova, M. O'Keeffe and O. M. Yaghi, *Science*, 2013, **341**, 974-+.
7. V. V. Butova, M. A. Soldatov, A. A. Guda, K. A. Lomachenko and C. Lamberti, *Russ. Chem. Rev.*, 2016, **85**, 280-307.
8. Z. Q. Wang and S. M. Cohen, *Chem. Soc. Rev.*, 2009, **38**, 1315-1329.
9. K. K. Tanabe and S. M. Cohen, *Chem. Soc. Rev.*, 2011, **40**, 498-519.
10. D. Zhao, D. J. Timmons, D. Q. Yuan and H. C. Zhou, *Accounts Chem. Res.*, 2011, **44**, 123-133.
11. S. M. Cohen, *Chem. Rev.*, 2012, **112**, 970-1000.
12. F. A. A. Paz, J. Klinowski, S. M. F. Vilela, J. P. C. Tome, J. A. S. Cavaleiro and J. Rocha, *Chem. Soc. Rev.*, 2012, **41**, 1088-1110.
13. W. G. Lu, Z. W. Wei, Z. Y. Gu, T. F. Liu, J. Park, J. Park, J. Tian, M. W. Zhang, Q. Zhang, T. Gentle, M. Bosch and H. C. Zhou, *Chem. Soc. Rev.*, 2014, **43**, 5561-5593.
14. J. D. Evans, C. J. Sumby and C. J. Doonan, *Chem. Soc. Rev.*, 2014, **43**, 5933-5951.
15. D. Farrusseng, S. Aguado and C. Pinel, *Angew. Chem.-Int. Edit.*, 2009, **48**, 7502-7513.
16. J. Lee, O. K. Farha, J. Roberts, K. A. Scheidt, S. T. Nguyen and J. T. Hupp, *Chem. Soc. Rev.*, 2009, **38**, 1450-1459.
17. L. Q. Ma, C. Abney and W. B. Lin, *Chem. Soc. Rev.*, 2009, **38**, 1248-1256.
18. A. Corma, H. Garcia and F. Xamena, *Chem. Rev.*, 2010, **110**, 4606-4655.
19. M. Ranocchiari and J. A. van Bokhoven, *Phys. Chem. Chem. Phys.*, 2011, **13**, 6388-6396.
20. A. Dhakshinamoorthy and H. Garcia, *Chem. Soc. Rev.*, 2012, **41**, 5262-5284.
21. M. Yoon, R. Srirambalaji and K. Kim, *Chem. Rev.*, 2012, **112**, 1196-1231.
22. F. Xamena and J. Gascon, *Metal Organic Frameworks as Heterogeneous Catalysts* Royal Soc. Chem., Cambridge, 2013.
23. J. W. Liu, L. F. Chen, H. Cui, J. Y. Zhang, L. Zhang and C. Y. Su, *Chem. Soc. Rev.*, 2014, **43**, 6011-6061.
24. A. H. Chughtai, N. Ahmad, H. A. Younus, A. Laypkov and F. Verpoort, *Chem. Soc. Rev.*, 2015, **44**, 6804-6849.
25. S. S. Y. Chui, S. M. F. Lo, J. P. H. Charmant, A. G. Orpen and I. D. Williams, *Science*, 1999, **283**, 1148-1150.
26. C. Prestipino, L. Regli, J. G. Vitillo, F. Bonino, A. Damin, C. Lamberti, A. Zecchina, P. L. Solari, K. O. Kongshaug and S. Bordiga, *Chem. Mat.*, 2006, **18**, 1337-1346.
27. S. Bordiga, L. Regli, F. Bonino, E. Groppo, C. Lamberti, B. Xiao, P. S. Wheatley, R. E. Morris and A. Zecchina, *Phys. Chem. Chem. Phys.*, 2007, **9**, 2676-2685.
28. F. Bonino, S. Chavan, J. G. Vitillo, E. Groppo, G. Agostini, C. Lamberti, P. D. C. Dietzel, C. Prestipino and S. Bordiga, *Chem. Mat.*, 2008, **20**, 4957-4968.
29. S. Chavan, J. G. Vitillo, E. Groppo, F. Bonino, C. Lamberti, P. D. C. Dietzel and S. Bordiga, *J. Phys. Chem. C*, 2009, **113**, 3292-3299.
30. P. D. C. Dietzel, P. A. Georgiev, J. Eckert, R. Blom, T. Strassle and T. Unruh, *Chem. Commun.*, 2010, **46**, 4962-4964.
31. E. D. Bloch, L. J. Murray, W. L. Queen, S. Chavan, S. N. Maximoff, J. P. Bigi, R. Krishna, V. K. Peterson, F. Grandjean, G. J. Long, B. Smit, S. Bordiga, C. M. Brown and J. R. Long, *J. Am. Chem. Soc.*, 2011, **133**, 14814-14822.
32. J. H. Cavka, S. Jakobsen, U. Olsbye, N. Guillou, C. Lamberti, S. Bordiga and K. P. Lillerud, *J. Am. Chem. Soc.*, 2008, **130**, 13850-13851.
33. L. Valenzano, B. Civalleri, S. Chavan, S. Bordiga, M. H. Nilsen, S. Jakobsen, K. P. Lillerud and C. Lamberti, *Chem. Mat.*, 2011, **23**, 1700-1718.
34. S. Chavan, J. G. Vitillo, D. Gianolio, O. Zavorotynska, B. Civalleri, S. Jakobsen, M. H. Nilsen, L. Valenzano, C. Lamberti, K. P. Lillerud and S. Bordiga, *Phys. Chem. Chem. Phys.*, 2012, **14**, 1614-1626.
35. S. Øien, D. Wragg, H. Reinsch, S. Svelle, S. Bordiga, C. Lamberti and K. P. Lillerud, *Cryst. Growth Des.*, 2014, **14**, 5370-5372.

36. G. C. Shearer, S. Chavan, J. Ethiraj, J. G. Vitillo, S. Svelle, U. Olsbye, C. Lamberti, S. Bordiga and K. P. Lillerud, *Chem. Mat.*, 2014, **26**, 4068-4071.
37. G. C. Shearer, S. Chavan, S. Bordiga, S. Svelle, U. Olsbye and K. P. Lillerud, *Chem. Mat.*, 2016, **28**, 3749-3761.
38. G. C. Shearer, J. G. Vitillo, S. Bordiga, S. Svelle, U. Olsbye and K. P. Lillerud, *Chem. Mat.*, 2016, **28**, 7190-7193.
39. K. E. deKrafft, W. S. Boyle, L. M. Burk, O. Z. Zhou and W. B. Lin, *J. Mater. Chem.*, 2012, **22**, 18139-18144.
40. S. Jakobsen, D. Gianolio, D. S. Wragg, M. H. Nilsen, H. Emerich, S. Bordiga, C. Lamberti, U. Olsbye, M. Tilset and K. P. Lillerud, *Phys. Rev. B*, 2012, **86**, Art. n. 125429.
41. A. M. Ebrahim and T. J. Bandosz, *ACS Appl. Mater. Interfaces*, 2013, **5**, 10565-10573.
42. M. Lammert, M. T. Wharmby, S. Smolders, B. Bueken, A. Lieb, K. A. Lomachenko, D. De Vos and N. Stock, *Chem. Commun.*, 2015, **51**, 12578-12581.
43. F. Nouar, M. I. Breeze, B. C. Campo, A. Vimont, G. Clet, M. Daturi, T. Devic, R. I. Walton and C. Serre, *Chem. Commun.*, 2015, **51**, 14458-14461.
44. R. Dalapati, B. Sakthivel, A. Dhakshinamoorthy, A. Buragohain, A. Bhunia, C. Janiak and S. Biswas, *Crystengcomm*, 2016, **18**, 7855-7864.
45. S. J. Garibay and S. M. Cohen, *Chem. Commun.*, 2010, **46**, 7700-7702.
46. M. Kandiah, S. Usseglio, S. Svelle, U. Olsbye, K. P. Lillerud and M. Tilset, *J. Mater. Chem.*, 2010, **20**, 9848-9851.
47. M. Kandiah, M. H. Nilsen, S. Usseglio, S. Jakobsen, U. Olsbye, M. Tilset, C. Larabi, E. A. Quadrelli, F. Bonino and K. P. Lillerud, *Chem. Mat.*, 2010, **22**, 6632-6640.
48. S. M. Chavan, G. C. Shearer, S. Svelle, U. Olsbye, F. Bonino, J. Ethiraj, K. P. Lillerud and S. Bordiga, *Inorg. Chem.*, 2014, **53**, 9509-9515.
49. J. Ethiraj, E. Albanese, B. Civalleri, J. G. Vitillo, F. Bonino, S. Chavan, G. C. Shearer, K. P. Lillerud and S. Bordiga, *ChemSusChem*, 2014, **7**, 3382-3388.
50. S. Chavan, J. G. Vitillo, M. J. Uddin, F. Bonino, C. Lamberti, E. Groppo, K. P. Lillerud and S. Bordiga, *Chem. Mat.*, 2010, **22**, 4602-4611.
51. C. Wang, K. E. deKrafft and W. B. Lin, *J. Am. Chem. Soc.*, 2012, **134**, 7211-7214.
52. P. H. Ling, J. P. Lei, L. Jia and H. X. Ju, *Chem. Commun.*, 2016, **52**, 1226-1229.
53. R. Kardanpour, S. Tangestaninejad, V. Mirkhani, M. Moghadam, I. Mohammadpoor-Baltork, A. R. Khosropour and F. Zadehahmadi, *J. Organomet. Chem.*, 2014, **761**, 127-133.
54. W. H. Dong, C. Feng, L. Zhang, N. Z. Shang, S. T. Gao, C. Wang and Z. Wang, *Catal. Lett.*, 2016, **146**, 117-125.
55. K. Tulig and K. S. Walton, *RSC Adv.*, 2014, **4**, 51080-51083.
56. J. Yang, L. T. Yang, H. L. Ye, F. Q. Zhao and B. Z. Zeng, *Electrochim. Acta*, 2016, **219**, 647-654.
57. Q. Q. Yuan, D. M. Zhang, L. van Haandel, F. Y. Ye, T. Xue, E. J. M. Hensen and Y. J. Guan, *J. Mol. Catal. A-Chem.*, 2015, **406**, 58-64.
58. E. Plessers, D. E. De Vos and M. B. J. Roeffaers, *J. Catal.*, 2016, **340**, 136-143.
59. S. Øien, G. Agostini, S. Svelle, E. Borfecchia, K. A. Lomachenko, L. Mino, E. Gallo, S. Bordiga, U. Olsbye, K. P. Lillerud and C. Lamberti, *Chem. Mat.*, 2015, **27**, 1042-1056.
60. L. Braglia, E. Borfecchia, L. Maddalena, S. Øien, K. A. Lomachenko, A. L. Bugaev, S. Bordiga, A. V. Soldatov, K. P. Lillerud and C. Lamberti, *Catal. Today*, 2017, **283**, 89-103.
61. F. Xamena, O. Casanova, R. G. Tailleur, H. Garcia and A. Corma, *J. Catal.*, 2008, **255**, 220-227.
62. A. Corma, M. Iglesias, F. Xamena and F. Sanchez, *Chem.-Eur. J.*, 2010, **16**, 9789-9795.
63. I. Luz, F. Xamena and A. Corma, *J. Catal.*, 2010, **276**, 134-140.
64. E. Borfecchia, D. Gianolio, G. Agostini, S. Bordiga and C. Lamberti, in *Metal Organic Frameworks as Heterogeneous Catalysts*, eds. F. Xamena and J. Gascon, Royal Soc Chemistry, Cambridge, 2013, pp. 143-208.
65. S. Bordiga, E. Groppo, G. Agostini, J. A. van Bokhoven and C. Lamberti, *Chem. Rev.*, 2013, **113**, 1736-1850.

66. K. C. Szeto, K. P. Lillerud, M. Tilset, M. Bjorgen, C. Prestipino, A. Zecchina, C. Lamberti and S. Bordiga, *J. Phys. Chem. B*, 2006, **110**, 21509-21520.
67. K. C. Szeto, C. Prestipino, C. Lamberti, A. Zecchina, S. Bordiga, M. Bjorgen, M. Tilset and K. P. Lillerud, *Chem. Mat.*, 2007, **19**, 211-220.
68. J. Hafizovic, M. Bjorgen, U. Olsbye, P. D. C. Dietzel, S. Bordiga, C. Prestipino, C. Lamberti and K. P. Lillerud, *J. Am. Chem. Soc.*, 2007, **129**, 3612-3620.
69. S. Chavan, F. Bonino, J. G. Vitillo, E. Groppo, C. Lamberti, P. D. C. Dietzel, A. Zecchina and S. Bordiga, *Phys. Chem. Chem. Phys.*, 2009, **11**, 9811-9822.
70. S. Bordiga, F. Bonino, K. P. Lillerud and C. Lamberti, *Chem. Soc. Rev.*, 2010, **39**, 4885-4927.
71. E. Borfecchia, S. Maurelli, D. Gianolio, E. Groppo, M. Chiesa, F. Bonino and C. Lamberti, *J. Phys. Chem. C*, 2012, **116**, 19839-19850.
72. L. Valenzano, J. G. Vitillo, S. Chavan, B. Civalleri, F. Bonino, S. Bordiga and C. Lamberti, *Catalysis Today*, 2012, **182**, 67-79.
73. E. Borfecchia, L. Braglia, F. Bonino, S. Bordiga, S. Øien, U. Olsbye, K. P. Lillerud, J. A. van Bokhoven, K. A. Lomachenko, A. A. Guda, A. V. Soldatov and C. Lamberti, in *XAFS Techniques for Catalysts, Nanomaterials, and Surfaces*, eds. Y. Iwasawa, K. Asakura and M. Tada, Springer, Berlin, 2017, pp. 397-430.
74. M. Muller, S. Hermes, K. Kaehler, M. W. E. van den Berg, M. Muhler and R. A. Fischer, *Chem. Mat.*, 2008, **20**, 4576-4587.
75. E. D. Bloch, D. Britt, C. Lee, C. J. Doonan, F. J. Uribe-Romo, H. Furukawa, J. R. Long and O. M. Yaghi, *J. Am. Chem. Soc.*, 2010, **132**, 14382-14384.
76. S. Gross and M. Bauer, *Adv. Funct. Mater.*, 2010, **20**, 4026-4047.
77. T. B. Celic, M. Rangus, K. Lazar, V. Kaucic and N. Z. Logar, *Angew. Chem.-Int. Edit.*, 2012, **51**, 12490-12494.
78. T. H. Zhou, Y. H. Du, A. Borgna, J. D. Hong, Y. B. Wang, J. Y. Han, W. Zhang and R. Xu, *Energy Environ. Sci.*, 2013, **6**, 3229-3234.
79. M. Carboni, Z. K. Lin, C. W. Abney, T. Zhang and W. B. Lin, *Chem.-Eur. J.*, 2014, **20**, 14965-14970.
80. X. L. Li, Z. Y. Guo, C. X. Xiao, T. W. Goh, D. Tesfagaber and W. Y. Huang, *ACS Catal.*, 2014, **4**, 3490-3497.
81. C. X. Xiao, T. W. Goh, K. Brashler, Y. C. Pei, Z. Y. Guo and W. Y. Huang, *J. Phys. Chem. B*, 2014, **118**, 14168-14176.
82. Z. Y. Zhang, H. Yoshikawa and K. Awaga, *J. Am. Chem. Soc.*, 2014, **136**, 16112-16115.
83. D. R. Sun, F. X. Sun, X. Y. Deng and Z. H. Li, *Inorg. Chem.*, 2015, **54**, 8639-8643.
84. M. Du, L. Li, M. X. Li and R. Si, *RSC Adv.*, 2016, **6**, 62705-62716.
85. J. Ethiraj, F. Bonino, J. G. Vitillo, K. A. Lomachenko, C. Lamberti, H. Reinsch, K. P. Lillerud and S. Bordiga, *ChemSusChem*, 2016, **9**, 713-719.
86. Z. G. Hu, J. J. Lin, N. Ogiwara, A. Rodriguez, Y. W. Peng, Y. X. Wang, S. Horike and D. Zhao, *Crystengcomm*, 2016, **18**, 2803-2807.
87. A. S. Munn, F. Millange, M. Frigoli, N. Guillou, C. Falaise, V. Stevenson, C. Volkringer, T. Loiseau, G. Cibin and R. I. Walton, *Crystengcomm*, 2016, **18**, 8108-8114.
88. N. C. Thacker, Z. K. Lin, T. Zhang, J. C. Gilhula, C. W. Abney and W. B. Lin, *J. Am. Chem. Soc.*, 2016, **138**, 3501-3509.
89. G. Wang, K. Leus, S. Couck, P. Tack, H. Depauw, Y. Y. Liu, L. Vincze, J. F. M. Denayer and P. Van der Voort, *Dalton Trans.*, 2016, **45**, 9485-9491.
90. D. Yang, S. O. Odoh, J. Borycz, T. C. Wang, O. K. Farha, J. T. Hupp, C. J. Cramer, L. Gagliardi and B. C. Gates, *ACS Catal.*, 2016, **6**, 235-247.
91. G. M. Sheldrick, *Acta Crystallogr. Sect. A*, 2015, **71**, 3-8.
92. G. M. Sheldrick, *Acta Crystallogr. Sect. C-Struct. Chem.*, 2015, **71**, 3-8.
93. O. V. Dolomanov, L. J. Bourhis, R. J. Gildea, J. A. K. Howard and H. Puschmann, *J. Appl. Crystallogr.*, 2009, **42**, 339-341.

94. C. C. Wang, *Acta Crystallogr. Sect. E.-Struct Rep. Online*, 2009, **65**, O2081-U1362.
95. A. Schaate, P. Roy, A. Godt, J. Lippke, F. Waltz, M. Wiebcke and P. Behrens, *Chem.-Eur. J.*, 2011, **17**, 6643-6651.
96. S. Carlson, M. Clausen, L. Gridneva, B. Sommarin and C. Svensson, *J. Synchrot. Radiat.*, 2006, **13**, 359-364.
97. C. Lamberti, C. Prestipino, S. Bordiga, G. Berlier, G. Spoto, A. Zecchina, A. Laloni, F. La Manna, F. D'Anca, R. Felici, F. D'Acapito and P. Roy, *Nucl. Instrum. Methods Phys. Res. Sect. B-Beam Interact. Mater. Atoms*, 2003, **200**, 196-201.
98. B. Ravel and M. Newville, *J. Synchrot. Radiat.*, 2005, **12**, 537-541.
99. M. Newville, *J. Synchrot. Radiat.*, 2001, **8**, 322-324.
100. S. I. Zabinsky, J. J. Rehr, A. Ankudinov, R. C. Albers and M. J. Eller, *Phys. Rev. B*, 1995, **52**, 2995-3009.
101. J. J. Rehr and R. C. Albers, *Rev. Mod. Phys.*, 2000, **72**, 621-654.
102. M. Reiher, O. Salomon and B. A. Hess, *Theor. Chem. Acc.*, 2001, **107**, 48-55.
103. C. F. Guerra, J. G. Snijders, G. te Velde and E. J. Baerends, *Theor. Chem. Acc.*, 1998, **99**, 391-403.
104. G. te Velde, F. M. Bickelhaupt, E. J. Baerends, C. F. Guerra, S. J. A. Van Gisbergen, J. G. Snijders and T. Ziegler, *J. Comput. Chem.*, 2001, **22**, 931-967.
105. M. Lersch and M. Tilset, *Chem. Rev.*, 2005, **105**, 2471-2526.
106. R. A. Periana, D. J. Taube, S. Gamble, H. Taube, T. Satoh and H. Fujii, *Science*, 1998, **280**, 560-564.
107. D. Wolf, *Angew. Chem.-Int. Edit.*, 1998, **37**, 3351-3353.
108. R. Palkovits, M. Antonietti, P. Kuhn, A. Thomas and F. Schüth, *Angew. Chem.-Int. Edit.*, 2009, **48**, 6909-6912.
109. R. Palkovits, C. von Malotki, M. Baumgarten, K. Mullen, C. Baltes, M. Antonietti, P. Kuhn, J. Weber, A. Thomas and F. Schüth, *ChemSusChem*, 2010, **3**, 277-282.
110. M. Soorholtz, R. J. White, T. Zimmermann, M. M. Titirici, M. Antonietti, R. Palkovits and F. Schüth, *Chem. Commun.*, 2013, **49**, 240-242.
111. G. W. Stinton and J. S. O. Evans, *J. Appl. Crystallogr.*, 2007, **40**, 87-95.
112. G. Agostini, C. Lamberti, L. Palin, M. Milanesio, N. Danilina, B. Xu, M. Janousch and J. A. van Bokhoven, *J. Am. Chem. Soc.*, 2010, **132**, 667-678.
113. G. Bunker, *Introduction to XAFS A Practical Guide to X-ray Absorption Fine Structure Spectroscopy*, Cambridge University Press, Cambridge, 2010.
114. M. D. Hall, G. J. Foran, M. Zhang, P. J. Beale and T. W. Hambley, *J. Am. Chem. Soc.*, 2003, **125**, 7524-7525.
115. H. Yoshida, S. Nonoyama, Y. Yazawa and T. Hattori, *Phys. Scr.*, 2005, **T115**, 813-815.
116. E. Borfecchia, S. Oien, S. Svelle, L. Mino, L. Braglia, G. Agostini, E. Gallo, K. A. Lomachenko, S. Bordiga, A. A. Guda, M. A. Soldatov, A. V. Soldatov, U. Olsbye, K. P. Lillerud, C. Lamberti and Iop, *J. Phys.: Conf.Ser.*, 2016, **712**, Art. n. 012125.
117. S. A. Guda, A. A. Guda, M. A. Soldatov, K. A. Lomachenko, A. L. Bugaev, C. Lamberti, W. Gawelda, C. Bressler, G. Smolentsev, A. V. Soldatov and Y. Joly, *J. Chem. Theory Comput.*, 2015, **11**, 4512-4521.
118. G. Berlier, G. Spoto, S. Bordiga, G. Ricchiardi, P. Fisicaro, A. Zecchina, I. Rossetti, E. Selli, L. Forni, E. Giamello and C. Lamberti, *J. Catal.*, 2002, **208**, 64-82.
119. G. Berlier, G. Spoto, P. Fisicaro, S. Bordiga, A. Zecchina, E. Giamello and C. Lamberti, *Microchem J.*, 2002, **71**, 101-116.
120. A. Zecchina, M. Rivallan, G. Berlier, C. Lamberti and G. Ricchiardi, *Phys. Chem. Chem. Phys.*, 2007, **9**, 3483-3499.
121. A. I. Frenkel, *J. Synchrot. Radiat.*, 1999, **6**, 293-295.
122. A. I. Frenkel, C. W. Hills and R. G. Nuzzo, *J. Phys. Chem. B*, 2001, **105**, 12689-12703.
123. D. Glasner and A. I. Frenkel, in *X-Ray Absorption Fine Structure-XAFS13*, eds. B. Hedman and P. Painetta, Amer Inst Physics, Melville, 2007, vol. 882, pp. 746-748.

124. G. Agostini, R. Pellegrini, G. Leofanti, L. Bertinetti, S. Bertarione, E. Groppo, A. Zecchina and C. Lamberti, *J. Phys. Chem. C*, 2009, **113**, 10485-10492.
125. G. Agostini, A. Piovano, L. Bertinetti, R. Pellegrini, G. Leofanti, E. Groppo and C. Lamberti, *J. Phys. Chem. C*, 2014, **118**, 4085-4094.
126. B. Abecassis, F. Testard, O. Spalla and P. Barboux, *Nano Lett.*, 2007, **7**, 1723-1727.
127. J. Polte, T. T. Ahner, F. Delissen, S. Sokolov, F. Emmerling, A. F. Thunemann and R. Kraehnert, *J. Am. Chem. Soc.*, 2010, **132**, 1296-1301.
128. E. Groppo, G. Agostini, A. Piovano, N. B. Muddada, G. Leofanti, R. Pellegrini, G. Portale, A. Longo and C. Lamberti, *J. Catal.*, 2012, **287**, 44-54.
129. G. Agostini, C. Lamberti, R. Pellegrini, G. Leofanti, F. Giannici, A. Longo and E. Groppo, *ACS Catal.*, 2014, **4**, 187-194.
130. E. Groppo, G. Agostini, E. Borfecchia, L. Wei, F. Giannici, G. Portale, A. Longo and C. Lamberti, *J. Phys. Chem. C*, 2014, **118**, 8406-8415.
131. N. T. K. Thanh, N. Maclean and S. Mahiddine, *Chem. Rev.*, 2014, **114**, 7610-7630.
132. E. Groppo, G. Agostini, E. Borfecchia, A. Lazzarini, W. Liu, C. Lamberti, F. Giannici, G. Portale and A. Longo, *ChemCatChem*, 2015, **7**, 2188-2195.
133. P. Kluth, B. Johannessen, G. J. Foran, D. J. Cookson, S. M. Kluth and M. C. Ridgway, *Phys. Rev. B*, 2006, **74**, 9.
134. L. Guczi, A. Beck, A. Horvath, Z. Koppany, G. Stefler, K. Frey, I. Sajo, O. Geszti, D. Bazin and J. Lynch, *J. Mol. Catal. A-Chem.*, 2003, **204**, 545-552.
135. A. Witkowska, A. Di Cicco and E. Principi, *Phys. Rev. B*, 2007, **76**, 12.
136. G. Turnes Palomino, P. Fisicaro, S. Bordiga, A. Zecchina, E. Giamello and C. Lamberti, *J. Phys. Chem. B*, 2000, **104**, 4064-4073.
137. F. X. Llabrés i Xamena, P. Fisicaro, G. Berlier, A. Zecchina, G. Turnes Palomino, C. Prestipino, S. Bordiga, E. Giamello and C. Lamberti, *J. Phys. Chem. B*, 2003, **107**, 7036-7044.
138. M. Benfatto, P. D'Angelo, S. Della Longa and N. V. Pavel, *Phys. Rev. B*, 2002, **65**, Art. n 174205.
139. E. M. Alayon, M. Nachtegaal, M. Ranocchiari and J. A. van Bokhoven, *Chem. Commun.*, 2012, **48**, 404-406.
140. F. Giordanino, E. Borfecchia, K. A. Lomachenko, A. Lazzarini, G. Agostini, E. Gallo, A. V. Soldatov, P. Beato, S. Bordiga and C. Lamberti, *J. Phys. Chem. Lett.*, 2014, **5**, 1552-1559.
141. E. Borfecchia, K. A. Lomachenko, F. Giordanino, H. Falsig, P. Beato, A. V. Soldatov, S. Bordiga and C. Lamberti, *Chem. Sci.*, 2015, **6**, 548-563.
142. C. Lamberti, C. Prestipino, F. Bonino, L. Capello, S. Bordiga, G. Spoto, A. Zecchina, S. D. Moreno, B. Cremaschi, M. Garilli, A. Marsella, D. Carmello, S. Vidotto and G. Leofanti, *Angew. Chem.-Int. Edit.*, 2002, **41**, 2341-2344.
143. N. B. Muddada, U. Olsbye, L. Caccialupi, F. Cavani, G. Leofanti, D. Gianolio, S. Bordiga and C. Lamberti, *Phys. Chem. Chem. Phys.*, 2010, **12**, 5605-5618.
144. L. S. Kau, D. J. Spirasolomon, J. E. Pennerhahn, K. O. Hodgson and E. I. Solomon, *J. Am. Chem. Soc.*, 1987, **109**, 6433-6442.
145. M. H. Groothaert, J. A. van Bokhoven, A. A. Battiston, B. M. Weckhuysen and R. A. Schoonheydt, *J. Am. Chem. Soc.*, 2003, **125**, 7629-7640.
146. G. Kresse and J. Furthmuller, *Comput. Mater. Sci.*, 1996, **6**, 15-50.
147. G. Kresse and J. Furthmuller, *Phys. Rev. B*, 1996, **54**, 11169-11186.
148. L. Braglia, E. Borfecchia, K. A. Lomachenko, S. Oien, K. P. Lillerud, C. Lamberti and Iop, *J. Phys. Conf. Ser.*, 2016, **712**, Art, n. 012053.